DOI: 10.1002/adem.201180027

Battle in the Amazon: Arapaima versus Piranha**

By *M. A. Meyers,* Y. S. Lin, E. A. Olevsky* and *P.-Y. Chen*

The scales of the Arapaimas, a large freshwater fish (up to 200 kg), are a superb example of a natural material that has evolved to provide protection against predators. The Arapaimas lives primarily in Amazon basin lakes that become infested with piranhas as the dry season advances and is covered with scales having up to 10 cm length. They have a collagen interior with a highly mineralized external layer. The collagen fibers form a cross-lamellar arrangement which produces a laminate composite. The internal collagenous layer provides the flexibility to the scales, which can undergo significant elastic deformation prior to failure, providing considerable toughness. The mineralized exterior provides the required protection against predation. The flexibility of the biomineral is enabled by two factors: (i) a corrugated configuration in which the tensile strains are minimized; (ii) a graded composition. We propose herein that the structure of the scales, a composite consisting of a mineralized external layer with surface corrugations and an internal flexible collagenous foundation, can serve as inspiration for the design of flexible composites having a hard ceramic surface. The piranha (Serrasalminae) is one of the principal predators in seasonal lakes, in which fish get trapped. Its teeth form triangular arrays creating a guillotine action that is highly effective in slicing through muscle. The bite force is calculated for a piranha with a mass of 1 kg from estimated maximum force values applied by three muscle groups connecting the jaw to the mandible: it is ≈20 N. Mechanical tests on the scales and teeth demonstrate that the cutting and puncturing ability of the piranha teeth cannot penetrate the Arapaimas scales.

Biological materials exhibit complex architectures and hierarchically organized structures. The best example, the nacreous component of the abalone shell, has already successfully inspired a ceramic–polymer composite with outstanding toughness.[1,2]

Bruet *et al*.[3] have recently demonstrated that *Polypterus senegalus*, living in estuaries and muddy bottoms in Africa, has a multilayered dermal armor. Following this, Song *et al*.[4] analyzed the threat protection mechanisms offered by the dermal layer of *P. senegalus* against biting attacks from the same species. In this paper, we analyze the *Arapaimas* (genus) *gigas* (specie), one of the largest freshwater fish, reaching a length of 2.5 m and a mass of 200 kg (Figure 1). There is only one previous study on the scales of the *Arapaimas*,[5] which belongs to the family of the *Osteoglossidae*. Fish with bony scales, *Ostracoderms*, evolved in the Ordovician, about 500 million years ago. The literature on dermal scales of fish is rather scarce, but the consensus is that it serves the important purpose of protection from predators. The *Arapaimas* live primarily in seasonal lakes in the Amazon basin, populated by over 30 species of piranhas (family: *Characidae*; sub-family: *serrasalminae*). Among these, the most predatorial is the red piranha (*Pygocentrus natteri*). As the waters of the rivers recede during the dry season, both *Arapaimas* and piranha become trapped in the lakes and the latter eventually attack every bird, mammal, reptile (except alligators), or fish. However, the *Arapaimas* thrive in this environment. The motivation for this

[*] *Dr. M. A. Meyers, Y. S. Lin, P.-Y. Chen*
Department of Mechanical and Aerospace Engineering, University of California, San Diego, La Jolla, California, USA
E-mail: mameyers@ucsd.edu
Dr. M. A. Meyers
Department Nanoengineering, University of California, San Diego, La Jolla, California, USA
Y. S. Lin, and E. A. Olevsky
Department of Mechanical Engineering, San Diego State University, San Diego, California, USA
P.-Y. Chen
Department of Materials Science and Engineering, National Tsing Hua University, Hsinchu 30013, Taiwan, R.O.C.

[**] *The authors thank Gaspar Ritter, Kuryala Lodge, Araguaia, for providing us the Araipamas scales and Marcel de Roure for making all the contacts that made this possible. Without proper specimens this research could not have been conducted. Discussions with Prof. J. McKittrick are gratefully acknowledged. This research was funded by NSF DMR Biomaterials Program (Grant DMR 0510138).*

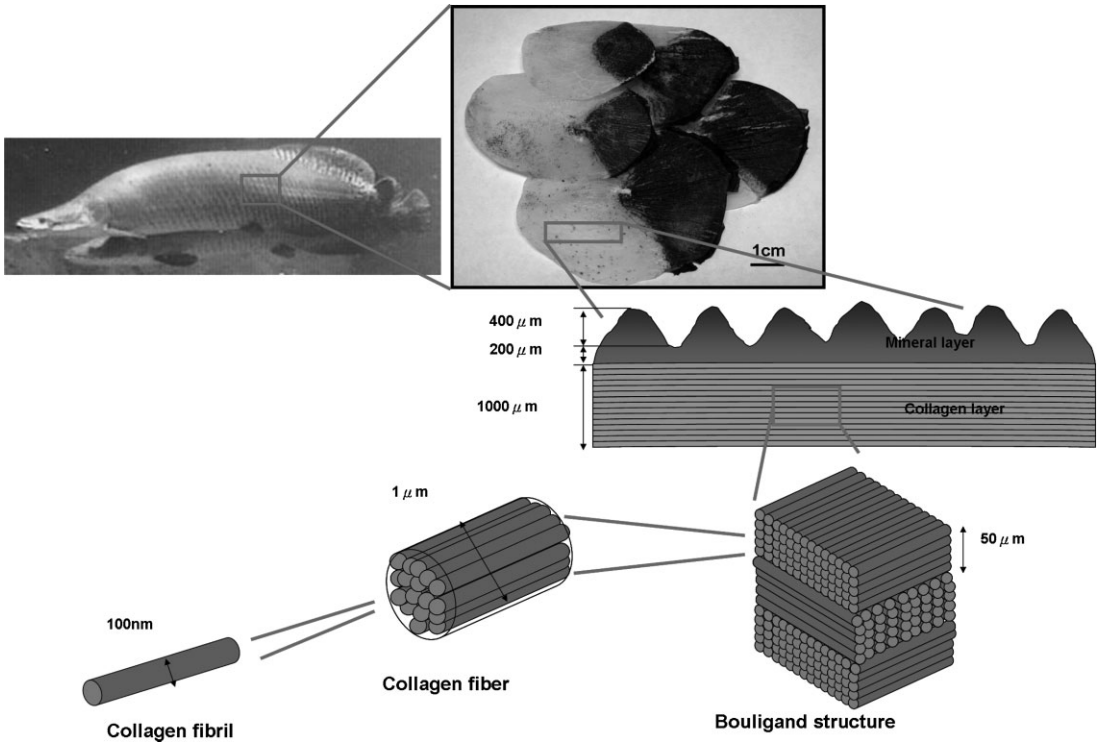

Fig. 1. Hierarchical structure of Arapaimas scales[31] (adapted from Lin et al.[15]) (Arapaimas photo by Melfi[34]).

study was to establish the reason how the *Arapaimas* and piranhas coexist. This entailed determining whether the scales of the *Arapaimas* provide effective protection against piranha teeth.

1. Experimental Procedures Structure and Properties of Arapaimas *Scales*

The scales were received from the Araguaia River, Brazil, and were rehydrated by inserting them in water for several days. This ensured complete hydration and was much longer than earlier measurements by Torres *et al.* [5]. We recognize the limitation of using dried and rehydrated scales but had no choice in this matter. Indeed, the scales show a pattern of cracks that is characteristic of the shrinkage associated with drying. Nevertheless, the material that cracked is not the fibers but the matrix between them. The red piranhas (*Pygocentrus natteri*) were brought from Brazil.

The specimens were imaged in an FEI-XL 30 Field Emission microscope operated at 20 kV accelerating voltage. Microhardness measurements were conducted in a LECO M-400-HI equipped with a Vickers indenter. A Hysitron TI 950 TriboIndenter was used to conduct the nanoindentation tests on piranha tooth. The piranha tooth was embedded in epoxy, ground with sand papers from 800 to 4000 grid, and polished with Al_2O_3 solution with particle size from 0.3 to 0.05 μm. A diamond Berkovich indenter was used to perform nanoindentation tests on the cross-section of the piranha tooth. All tests were performed in load-controlled feedback mode with various maximum loading forces. The loading function in the tests consists of 5-s loading to the peak force, followed by a 5-s hold segment, and 1-s unloading segment. The maximum load used is 1000 μN with a loading rate of $200\ \mu m \cdot s^{-1}$.

The penetration test was conducted in an Instron 3367. Several piranha teeth extracted from the piranha head were attached to the upper punch and the exposed and embedded parts of *Arapaimas* scale were fixed by glue on a synthetic rubber layer with a compressive elastic modulus of approximately 10 MPa attached to the lower punch. The piranha tooth penetrated into the scale with a crosshead velocity of $0.1\ mm \cdot min^{-1}$. In order to mimic the real condition, the rubber below the scale was used to simulate the soft tissue.

In order to reveal the collagen fibers, a demineralization procedure was applied by immersing the scales in 0.6 N HCl dilute from 1 N HCl for 5 days. For the deproteination procedure, the scale was immersed in 2.6% NaOCl for 7 days to remove the protein completely.

Fourier transform infrared spectroscopy (FTIR) was used to analyze the chemical compounds in the scale with different absorption peaks which correspond to different frequencies of vibration of atomic bonds. A sample with an area of $1\ cm^2$ was cut from the embedded part of the scale and polished to a thickness of 300 μm. A Varian Excalibur 3100 FTIR spectrometer with spectral resolution of $20\ cm^{-1}$ was used to identify the chemical compounds in the scale. The sample was tested in attenuated total reflectance (ATR) mode of Si and ZnSe plate equipped in the FTIR instrument.

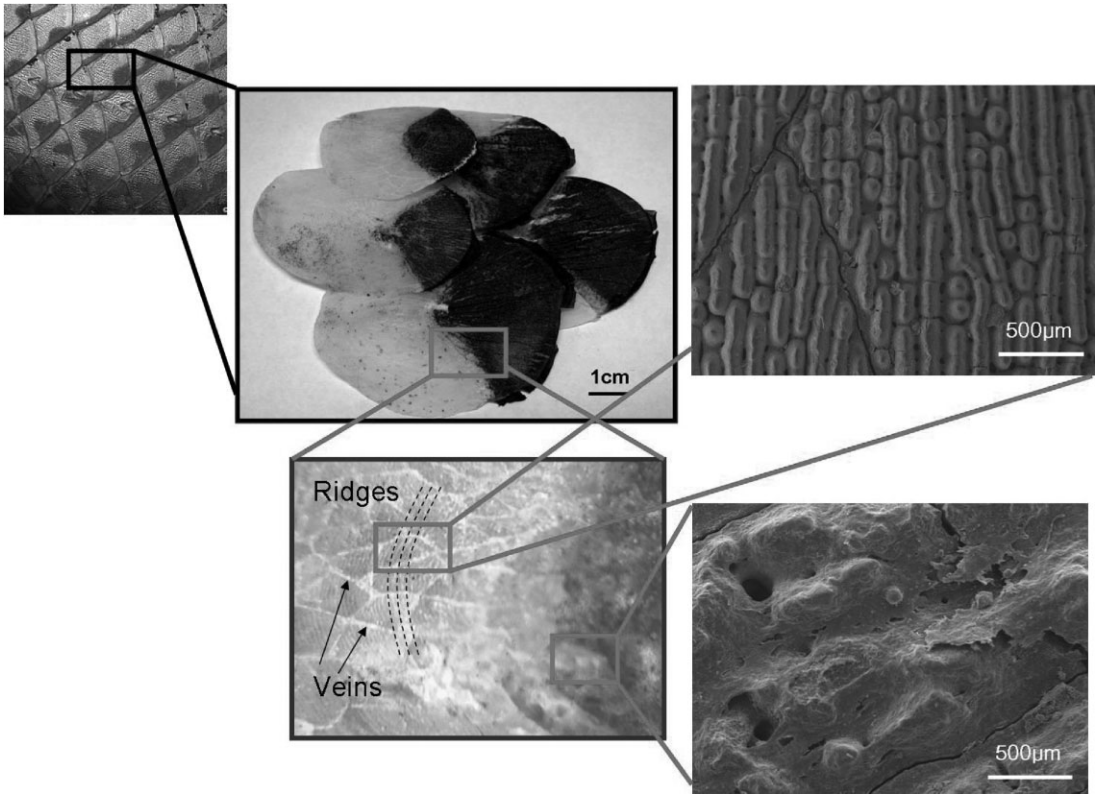

Fig. 2. Arapaimas scale at increasing magnifications; light (covered) on left and dark (exposed) region on right. Corrugations have a spacing of ≈200 μm for light and are larger than ≈500 μm for dark regions.

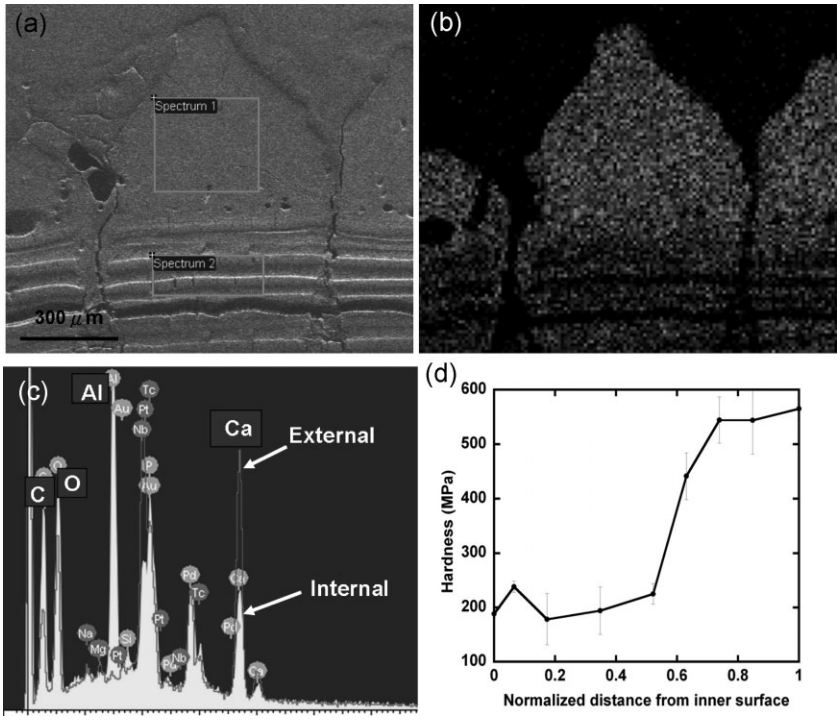

Fig. 3. (a) BSE image of scale cross-section; (b) X-ray mapping of calcium; (c) EDS analysis profile of two areas (external and internal) marked in SEM micrograph; (d) microhardness across the scale cross-section.

2. *Structure and Properties of* Arapaimas *Scales*

The *Arapaimas* scales are the largest of all freshwater fish, reaching a length of up to 10 cm. Like most fish scales,[6–13] they are composed of successive layers of collagen, forming a composite structure, as shown in Figure 1.[1] The surface is highly mineralized and has a corrugated appearance, which has led to its use by Amazon inhabitants as nail files. The corrugation edges are perpendicular to the long axis of the scales. Figure 2 (upper center) shows superposed scales with length of ≈10 cm each; the dark regions represent the exposed part of the scales. The scales form an overlapping pattern in such a manner that three layers cover most of the body. The light region (which overlaps) represents approximately 2/3 of the scale area. It consists of parallel ridges with spacing of approximately 200 μm; the exposed portion (dark gray) has ridges that have a larger scale (≈1 mm). This portion of the scale is also thicker (≈2 mm) and less flexible whereas the light region has a thickness half of that: ≈1 mm. This geometric

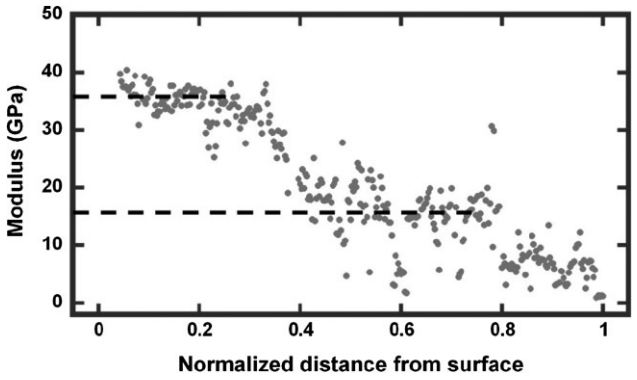

Fig. 4. Reduced modulus from nanoindentation hardness measurements on cross-section of scale (from Chen et al.[33]).

relationship between the two parts reduces irregularities on the surface of the fish, ensuring an interface in which water flow is laminar and reducing drag. Along the edge of the scale there is a thin flexible flap that ensures smoothness. The scale has veins, which can be seen in the right hand side of Figure 2.

The scans in Figure 3 confirm that the exposed layer of the scale is highly mineralized. Figure 3(a, b) show a cross-section perpendicular to the ridges. The peaks from the outside surface (thin lines) show the high calcium content whereas the ones from the inside (thin lines) do not show its presence in such a prominent manner. The large Al peak is due to the residual Al_2O_3 polishing solution that remained embedded in the cracks. The calcium is concentrated in the triangular ridges in Figure 3(a, b), which correspond to the corrugations shown schematically in Figure 1 and seen in the bottom view in Figure 2. This higher degree of mineralization of the outer layer is also reflected in a higher hardness, also shown in Figure 3(d). The microhardness changes in a graded manner from ≈200 to 600 MPa, strongly suggesting a gradient of biomineralization increasing toward the external surface of the scales. The mineral in the scale was identified through X-ray diffraction as hydroxyapatite. The significant broadening of the peaks suggests that the individual crystals are in the nanometer range, similar to bone.

The profile of Young's modulus obtained from nanoindentation measurements in Figure 4 shows, in a clear fashion, how the stiffness varies with distance from the external surface. The Young's modulus in the outside is in the range 30–40 GPa, while that in the inside, mostly collagenous layer, is approximately 15 GPa. These results, by Chen *et al.*[33] are somewhat lower but consistent with the ones obtained by Lin *et al.*[15]: $E_m = 46.8$ GPa, and $E_c = 16.7$ GPa, for the mineral and collagen, respectively. It should be mentioned that these measurements were made on dry specimens.

SEM observation of the scales reveals layers which, on closer examination, consist of collagen fibrils with diameters of ≈100 nm, Figure 5(a). The characteristic banding pattern with periodicity of 67 nm is seen. These collagen fibrils were revealed by demineralizing the scales. The scales also underwent a deproteination procedure to reveal the mineral.

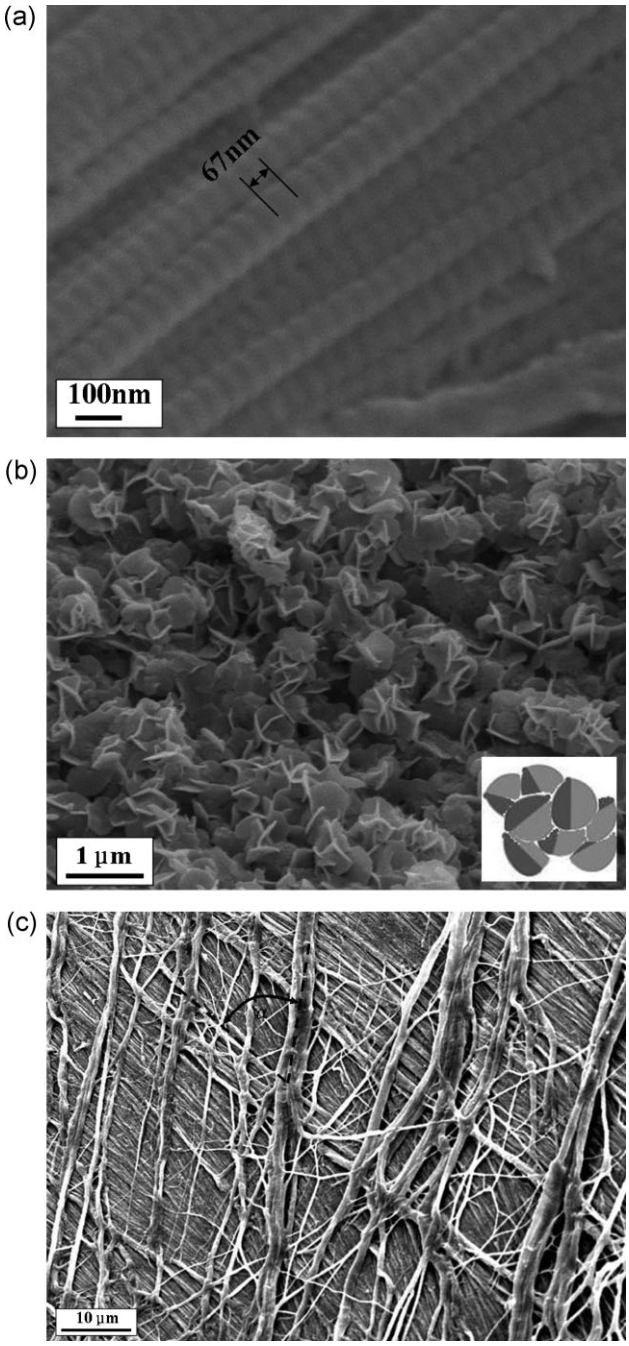

Fig. 5. (a) Fibrils observed after demineralization showing the 67-nm periodicity characteristic of collagen; (b) mineral platelets with different orientations observed after deproteination exhibiting a tri-leaf disks shape with thickness of 50 nm and diameter of 500 nm; (c) cross-lamellar structure of fibers viewed parallel to scale surface; angle $\alpha \approx 50–68°$.

The mineral platelets with random distribution can be seen in Figure 5(b). The minerals consist of platelets with thickness of ≈50 nm and diameter of ≈0.5 µm; often, these platelets are joined as three half disks along a common axis. The insert represents such an idealized arrangement. It is possible that these minerals were produced in the process of deproteinization. This is an area for further investigation.

The collagen fibrils form fibers which, on their turn, form bundles with diameters on the order of 1–5 μm. The latter are organized into lamellae with an average thickness of 50 μm.

Adjacent lamellae have the fibrils rotated at an angle of ≈60°. This is revealed in the SEM micrograph of Figure 5(c). Thus, the scale is a collagen composite laminate. This structure is analogous to that observed in other fish scales, apart from the dimensions. In *P. reticlata* (guppy), the lamellae are ≈1 μm thick; in *C. auratus* (goldfish), they are around 5 μm. The angles between layers have also been found to vary from 36° for teleosts,[7] to 90° for *P. major*,[6] to less than 90° for *H. bimaculatus*.[9]

Thus, the scale is a hierarchical composite adapted to the needs for survival: an interior which enables flexing covered with a corrugated mineralized layer. The exposed mineral portion of the scale is thicker (dark region in Figure 2) and has a higher degree of mineralization. The microhardness measured across the section of the scale reflects the higher mineralization on the outside. This is shown in Figure 3. The mineralized region's microhardness (≈600 MPa) is roughly three times that of the internal region. We also performed nanoindentation measurements to compare our results with the ones by Bruet *et al*.[3] Their values ranged from 0.54 to 4.5 GPa whereas our values varied from 0.6 (internal region) to 2 GPa (external region). The ganoine, present as the external layer of *P. senegalus*, clearly confers it the outstanding hardness, considerably higher than that of *Arapaimas*.

FTIR with ATR was conducted on the fish scale to identify the calcium phosphate phase. The results are similar to the previous studies (e.g.,[5]). The main absorption peaks, 1637, 1546, and 1239 cm^{-1} are the three characteristic peaks that correspond to amide I, amide II, and amide III of type I collagen. Peaks at around 1000 cm^{-1}, which represent the phosphate groups and 1872, 1401, 14 550 cm^{-1} which correspond to carbonate anions, were also observed. All of these peaks indicate that the scale is composed of an organic component (type I collagen) and an inorganic component (calcium-deficient hydroxyapatite).

Our study suggests that the corrugations in the mineralized layer have an important structural function. If the thickness of this layer were homogeneous, it would restrict the flexibility of the scale, which is necessary for gliding with minimum drag through water and to ensure that the scales are in intimate contact with the host. If a ceramic layer with constant thickness were strained to follow a curved shape, the mineral would crack. Figure 6 shows, in schematic fashion, how the flexing of the graded composite can be accomplished with minimum tensile strain in the mineral layer. The scale can be subjected to considerable flexure if the axis is parallel to the edges of the corrugations. The

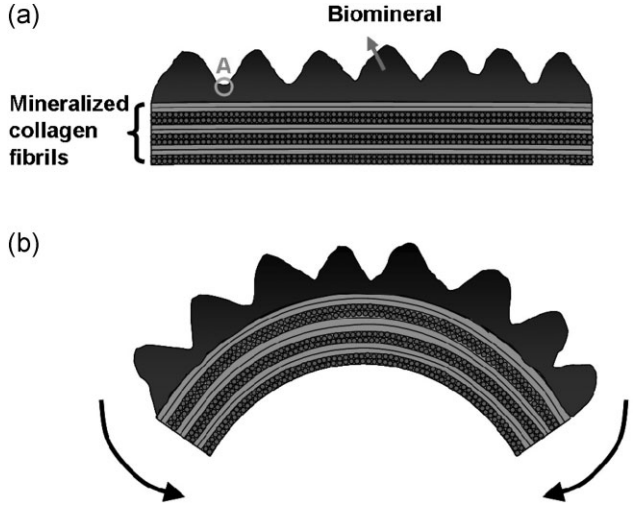

Fig. 6. Schematic representation of the flexing of the Arapaimas scale showing how the corrugations minimize the tensile strains in the mineralized layer, by providing channels in which the thickness is smaller. Circled region A undergoes minimum strain by virtue of geometry. (a) Extended (normal) and (b) flexed configurations.

presence of the corrugations ensures that the strain is concentrated at their bottoms (region marked A in Figure 6). This is an important observation which will be discussed further in Section 5.

It is possible to estimate the decrease in tensile stresses in the ceramic layer by the introduction of the corrugated layer. This is shown below using mechanics of materials principles, as explained by Popov,[14] among others. The procedure used to estimate the maximum tensile stresses is to transform the external ceramic layer by using the ratios between the elastic constants. Figure 7 shows longitudinal views of two configurations of composite beams (E_m, mineral elastic modulus; E_c,

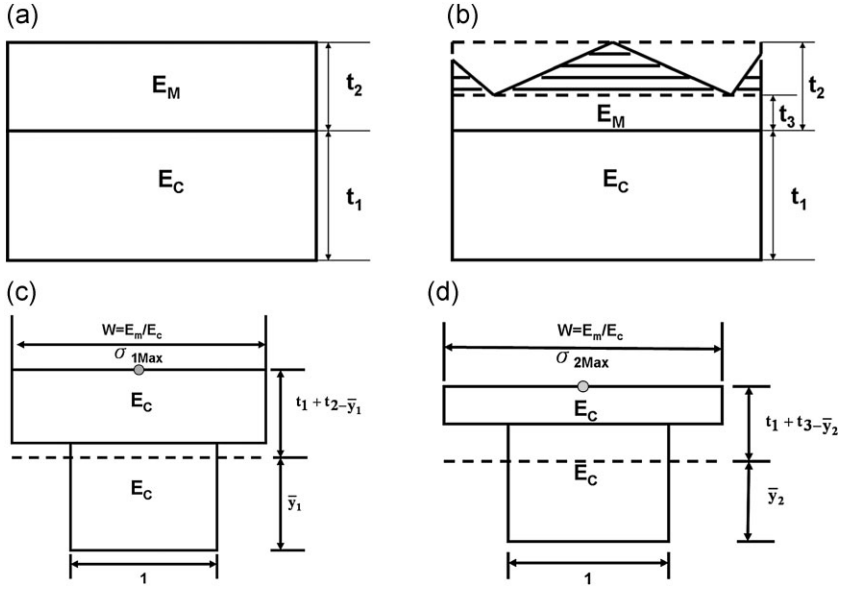

Fig. 7. Longitudinal section of the Arapaima scale; (a) fully mineralized surface layer. (b) Corrugated mineral layer. Cross-section of transformed beams for (c) smooth and (d) corrugated mineral layers; neutral axis marked by $\bar{y}$.

collagen elastic modulus): (i) one with a constant mineral thickness and (ii) with a variable thickness that is represented by triangles. The thicknesses of the layers are marked in Figure 7. For the corrugated mineral layer, they can be obtained from microscopic measurements.

Figure 7(c, d) are the cross-sections of the transformed beams. The mineral part was transformed into an equivalent collagen section. For simplicity, the cross section was taken as uniform. This is a standard procedure, and the area of the mineral is transformed with the ratio of the elastic moduli, $E_m/E_c = n_m$.

We calculate the maximum stress on the mineral layers of these two composite beams under same deflection. And the results show that the maximum stress on the mineral layers of the composite beam with thin mineral layer are lower than for the composite beam with thick mineral layer. The following is the analysis of maximum stress on these two composite beams. We take the elastic modulus of the collagen layer as reference and transform the cross-section of the mineral layer into a larger area which has the same elastic modulus as collagen layer.

The maximum deflection of a beam deformed by a constant bending moment M is (page A-13,[14])

$$\delta = -\frac{ML^2}{9\sqrt{3}EI} \tag{1}$$

where L is the length of the beam, E the elastic modulus, and I is the moment of inertia. Assuming a same deflection for the two cases

$$\delta = \frac{M_1L^2}{9\sqrt{3}E_cI_1} = \frac{M_2L^2}{9\sqrt{3}E_cI_2} \Rightarrow \frac{M_1}{I_1} = \frac{M_2}{I_2} \tag{2}$$

The maximum stress, in the outermost fiber of the mineral region, is (page 301,[14])

$$\sigma_M = \frac{\sigma_C}{n_m} = \frac{M \times \bar{y}}{I}\frac{1}{n_m} \tag{3}$$

where $n_m = E_m/E_c$ and $\bar{y}$ is the distance from the bottom layer to the neutral axis.

$$\begin{aligned} \sigma_{1t\max} &= \frac{M_1 \times (t_1 + t_2 - \bar{y}_1)}{I_1 \times n_m} \\ \sigma_{2t\max} &= \frac{M_2 \times (t_1 + t_3 - \bar{y}_2)}{I_2 \times n_m} \end{aligned} \tag{4}$$

At the same deflection, the ratio between the maximum stresses is

$$\frac{\sigma_{1t\max}}{\sigma_{2t\max}} = \frac{(t_1 + t_2 - \bar{y}_1)}{(t_1 + t_3 - \bar{y}_2)} \tag{5}$$

We are able to estimate the distances $t_1 = 1000\,\mu m$, $t_2 = 600\,\mu m$, and $t_3 = 200\,\mu m$. This can be verified from Figure 1 and 3. The ratio n_m is ≈2.8 which is calculated from the elastic moduli of mineral and collagen layers from Lin *et al.*,[15] 46.8 and 16.7 GPa, respectively. The ordinates of the neutral axis $\bar{y}_1$ and $\bar{y}_2$ are calculated as following

$$\bar{y}_1 = \frac{2.8 \times 0.6 \times 1.3 + 1 \times 0.5}{2.8 \times 0.6 + 1 \times 1} = 1\,mm$$

$$\bar{y}_2 = \frac{2.8 \times 0.2 \times 1.1 + 1 \times 0.5}{2.8 \times 0.2 + 1 \times 1} = 0.7\,mm$$

Thus

$$\frac{\sigma_{1t\max}}{\sigma_{2t\max}} = \frac{(t_1 + t_2 - \bar{y}_1)}{(t_1 + t_3 - \bar{y}_2)} = \frac{1 + 0.6 - 1}{1 + 0.2 - 0.7} = 1.20 \tag{6}$$

The maximum compressive stresses for the two different mineral layer thicknesses are calculated in the same fashion: $\frac{\sigma_{1c,\max}}{\sigma_{2c,\max}} = \frac{\bar{y}_1}{\bar{y}_2} = \frac{10}{7} = 1.42$.

Thus, both the maximum tensile and compressive stresses in the scale are reduced by the presence of corrugations. In addition, the reduction in I, the moment of inertia, from $I_1(=0.160\,mm^4)$ to $I_2(=0.06\,mm^4)$, creates a greater flexibility, i.e., the bending moment required for a specific deflection is decreased. Equation 1 shows that the deflection, at a constant bending moment, is inversely proportional to I. Thus, the compliance of the corrugated scale is three times higher than that of the solid one, and there is a definite advantage form a mechanics point of view, in having corrugations.

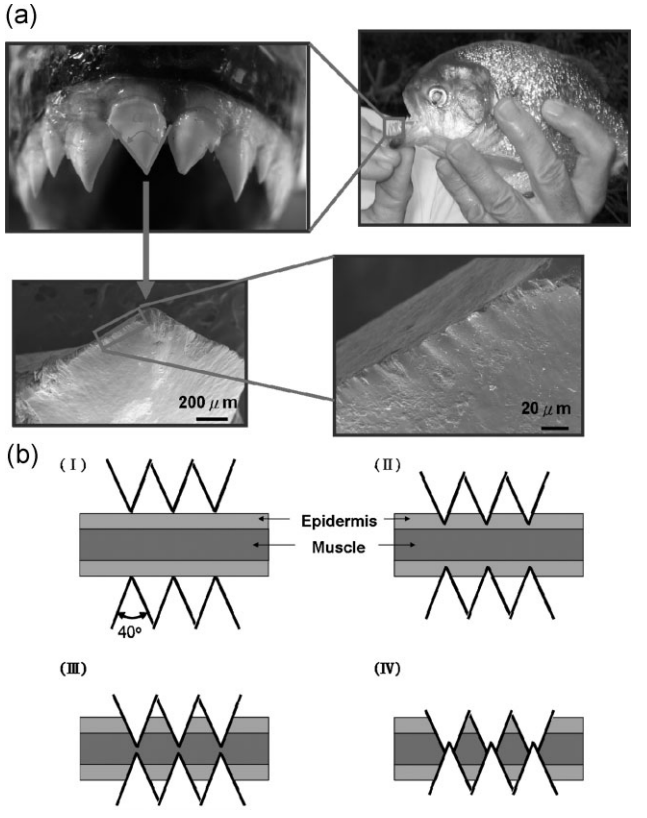

Fig. 8. (a) Red piranha mandible with teeth forming angle α_1 and details of teeth showing small serrations; (b) sequence of cutting by piranha teeth; epidermis and muscle are trapped by the guillotine effect.

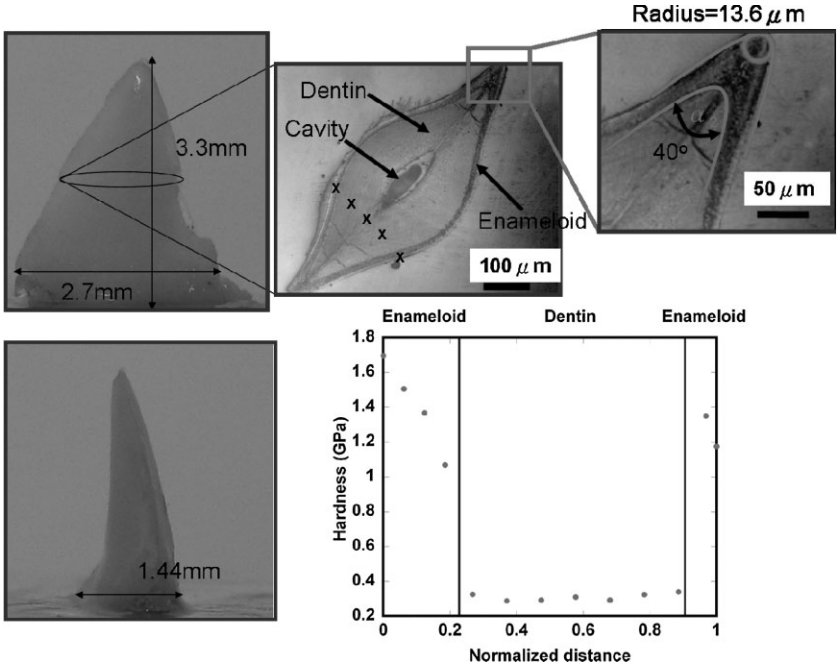

Fig. 9. Details of piranha tooth showing external enameloid layer covering a dentin interior; radius at the tip: 13.6 μm.

approximately 45°. Upon biting, the teeth produce a guillotine type effect that is highly efficient in cutting through soft tissue. This angle $\alpha_1 \approx 45^\circ$ ensures that the dermis and muscle are severed by an action providing both sliding and compression. Atkins [18,19] discusses the importance of both components in cutting of soft tissue.

The microhardness of the cross-section shows a significant rise on the outside, more highly mineralized layer. This is shown in Figure 9 where one can see that there are two layers. This outside layer has been identified as enameloid.[17,19] Its hardness, ≈1.5 GPa, is about one half of that of mammal enamel. The thickness of the enameloid layer is ≈15 μm in comparison with human enamel which is, on the sides of teeth, ≈200 μm. It is interesting to note that the dentine/enamel thickness ratio is about 10 in human teeth; this ratio is about the same in the piranha tooth, suggesting that the architecture of the tooth is scale-independent.

Nanoindentation mapping was also conducted in the cross-section and the results are shown in Figure 10. A total of 700 indents were made with a spacing of 50 μm. Figure 10 (a) and (b) show the reduced modulus and nanohardness values, respectively. The reduced modulus increases from ≈20 GPa, in the dentin area, to ≈80 GPa in the enameloid area. The nano-indentation values increase from ≈1 to 4 GPa. These values are higher than the

3. Structure and Properties of Piranha Teeth

Figure 8 shows a piranha and details of its teeth. The teeth are triangular and sharp, as evidenced by the magnified views. There are small serrations along the teeth; these were described earlier.[16] The teeth form arrays with an angle, α_1, of

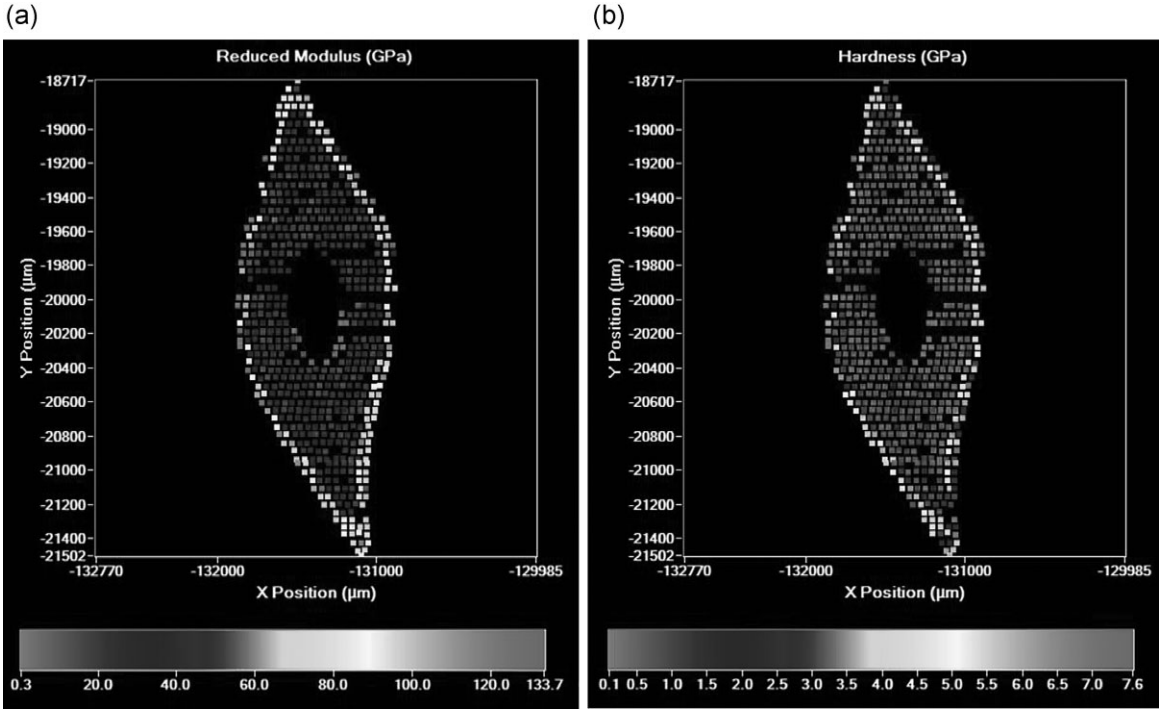

Fig. 10. Maps obtained from nanoindentation measurements on the cross-section of piranha tooth; (a) reduced modulus; (b) nanoindentation hardness. Modulus increases from 20 (in dentin) to 80 GPa in enameloid layer, whereas hardness increases from 1 to 4 GPa.

Table 1. Dimensional measurements on piranha mandible (mass ≈ 1000 g).

Muscle group	Angle	Segment length [mm]
	$\alpha_0 = 90^\circ$	AB = 6
A_1	$\alpha_1 = 10^\circ$	BC = 4
A_2	$\alpha_2 = 20^\circ$	CD = 5
A_3	$\alpha_3 = 70^\circ$	DE = 6

microindentation values, a feature often observed because of the scale of defects.[20]

Although experimental data on the bite force for piranha are non-existent to our knowledge, one can estimate it from the geometry of the maxilla and from the emplacement of the muscles using a calculational procedure developed by Westneat.[21] There are three principal muscle groups responsible for the bite in fish: A_1, A_2, and A_3. The muscle designations A_1, A_2, and A_3 are standard designations for fish mandibles.[21] Figure 11(a) shows the three muscle groups. In Figure 11(b) the biting action has been reduced to a free-body diagram. F, the biting force, is the unknown. The fulcrum represents the point around which the maxilla rotates. It is replaced by two force components F_{fx} and F_{fy} in Figure 11(b). The equations of equilibrium are

$$\sum M_E = F \cdot AE + F_{A_3}\cos\alpha_3 \cdot DE + F_{A_2}\cos\alpha_2 \cdot BE + F_{A_1}\cos\alpha_1 \cdot CE = 0 \quad (7)$$

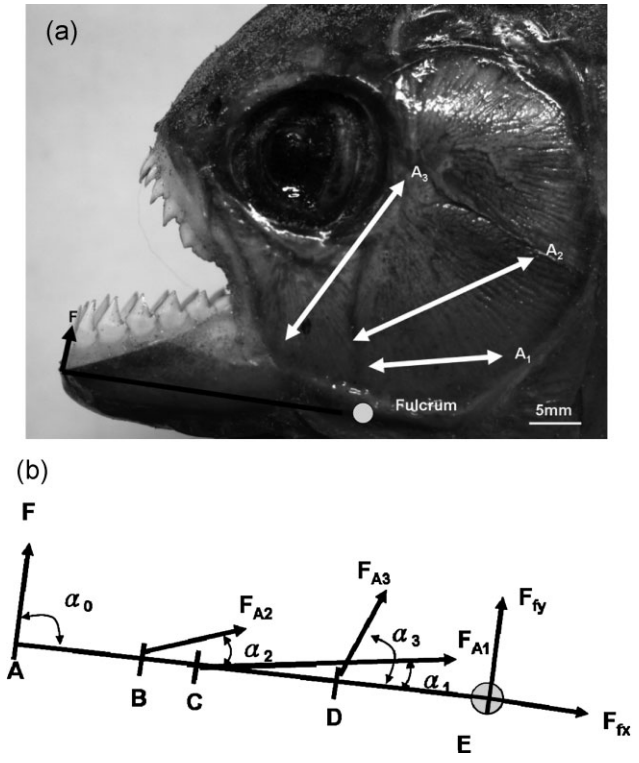

Fig. 11. (a) Side view of piranha head with emplacement of principal muscle groups and terminations; (b) free body diagram. Biting force F can be calculated from geometry and estimated values of F_{A_1}, F_{A_2}, and F_{A_3}.

Measured values of the angles and segments are given in Table 1. The estimated cross-sectional area of the muscles (≈100 mm^2 on each side) and the muscle force (200 $kN \cdot m^{-2}$) are used in the calculation. The muscle force is the highest value in the range indicated by Westneat[21] (100–200 $kN \cdot m^{-2}$).

The forces F_{A_1}, F_{A_2}, and F_{A_3} are estimated from the measurement of the maximum cross-sections of the three muscle groups. The calculated biting force for piranha is 17 N. Bite force measurements have been conducted for a number of fish species and this value is compatible with experimental results.[22–24,27] Although the bite force of the piranha is not large, the sharpness of the teeth is comparable to that of razor blades. Indeed, the radius of the tip, 13.6 μm, compares with values of 15–17 μm reported by Atkins for razor blades. The included angle, $\alpha_2 = 40^\circ$ (Figure 9) is much lower than the one in steel razor blades (15°) and closer to cutting knives (30–40°) because the compressive strength of the mineral is much lower than that of steel.[25,26] This radius of the tip explains the efficiency of piranha teeth in cutting through muscle. Song *et al.*[4] measured a similar value for *P. senegalus*: the radius of the tip had a mean of 11.7 μm while the angle $\alpha_2 = 44^\circ$ (in this case, a cone).

4. Penetration of Tooth into Scale

A piranha tooth was attached to a testing machine and advanced onto two regions of the *Araipamas* scale: covered (light) and exposed (dark). Figure 12 shows the load-penetration curves for the two cases: penetration into the covered (light) region [Figure 12(a)] as well as penetration into the exposed (dark) region [Figure 12(b)]. The stress–strain curves in compression for the synthetic rubber and for salmon meat are shown in Figure 12(c) and (d), respectively. Although the elastic modulus for rubber is fairly low, ≈10 MPA, it is still considerably higher than that for salmon. We did not have Arapaima meat to test and therefore do not know the compressive response of its muscle. The salmon muscle exhibits a J curve with an approximate modulus of 3 GPa. Several load-penetration curves are shown to illustrate the variation in response. On the right of the plots are photographs of typical loading sequences. The scales were fully hydrated prior to the penetration experiments and were placed on a rubber layer that simulated the underlying muscle. The initial force versus penetration response is linear for the two cases, with a slope of approximately 50 $N \cdot mm^{-1}$. This corresponds to the elastic flexing of the scale under the indentation force.

In Figure 12(a) the curves acquire a concavity that is indicative of penetration into the scale at loads of 25 N and higher. One of them shows a drop which suggests penetration. Figure 12(b) shows the same experiment applied to the external (dark) portion of the scale. Two loading curves show drops, marked by arrows; these designate fracture of the tooth. In other cases the tooth fractured but remained attached and penetration proceeded. However, upon unloading the fracture was revealed through the separation when the tooth is brought back to its original position. The photograph on the upper left-hand corner shows a broken tooth.

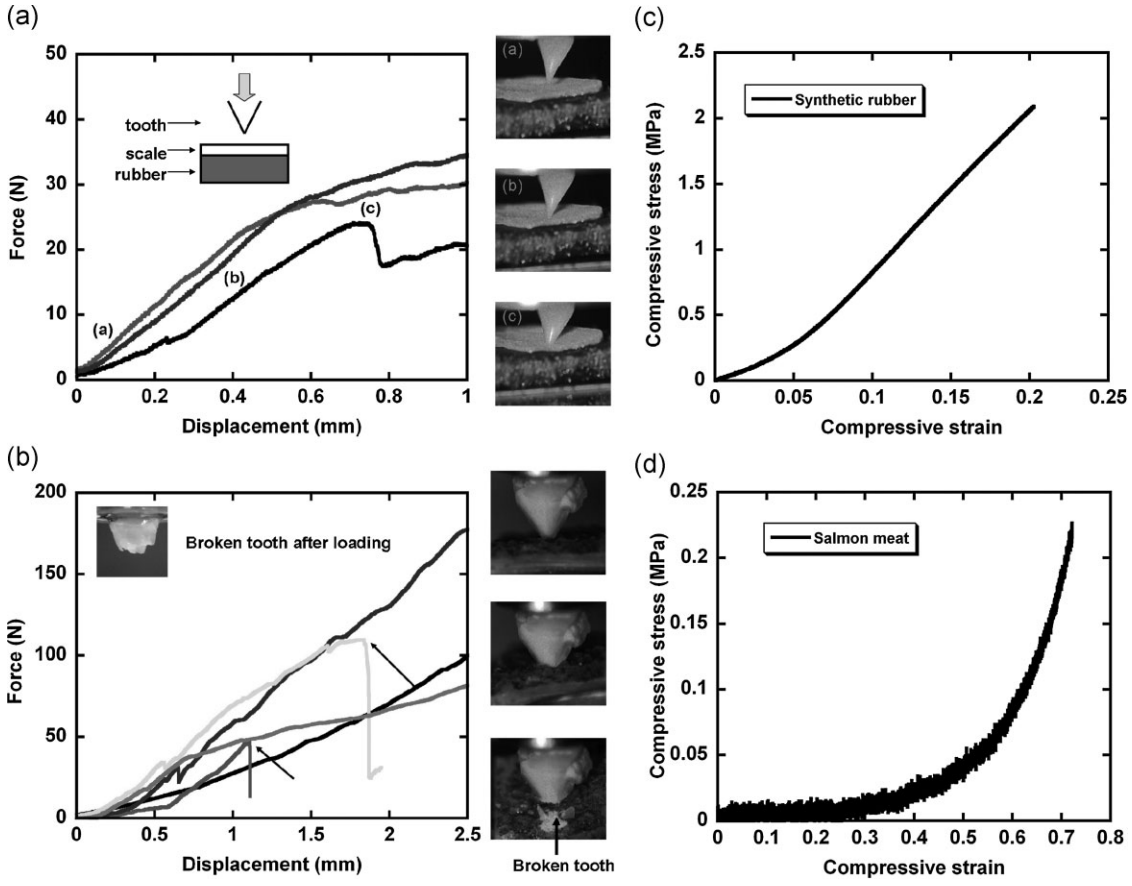

Fig. 12. (a) Force-penetration curves into internal region of Arapaimas scale by piranha tooth; (b) force-penetration curves into external region of scale; Tooth fracture indicated by arrows. Photographs on right-hand side illustrate different stages of tooth penetration into scale. (c, d) Stress–strain curves of synthetic rubber and salmon meat, respectively.

The hardness of the enamelous portion of the piranha tooth is significantly higher (≈1.5 GPa) than that of the mineralized surface of the scale (≈0.6 GPa). This explains the penetration capability of the tooth. Nevertheless, the strength of the tooth is exceeded for penetration into the dark region of the scale.

The thickness of the scale is ≈1 mm in the light (covered) region and ≈2 mm in the dark (exposed) region. Indeed, since the scales overlap, the piranha tooth would need to penetrate one dark layer and two light layers to enter into the muscle. This corresponds to ≈4 mm. The force required to penetrate 1 mm into the light layer is [Figure 12(a)] approximately equal to 30 N. The dark layer is more mineralized and thicker, and the resistance to penetration is higher. At a penetration of 1 mm, one has a force of approximately 50 N. The force increases with penetration in an approximately linear fashion. One can obtain the force required to penetrate through three layers (one dark and two light) layers by summing the forces required to penetrate into the dark layer by 4 mm, the force required to penetrate into a light layer by 2 mm and the last layer by1 mm. This total is approximately equal to: $120 + 60 + 30 = 210$ N.

The penetration results using a single piranha tooth can be used to extrapolate the force required for a full bite. The piranha engages the front teeth and we can reasonably assume the six teeth on each jaw are engaged. The total bite force required is: $210 \times 6 = 1260$ N. This number exceeds the bite force of a piranha by orders of magnitude. Thus, the experiments whose results are presented herein lead to a clear conclusion: the piranha bite cannot penetrate the *Arapaimas* scales.

5. Conclusions

The study of biological (or natural) materials is revealing a variety of new structures, mechanical responses and design principles that parallel and often exceed the ones of their synthetic counterparts. The reversible ''displacive'' transformation undergone by whelk eggs are a biological analog to the shape-memory effect;[28] the magnetite chiton radula is an example of an ultrahard ceramic (nanoindentation: 9–12 GPa) produced by a biomediated method;[29] the squid beak is an eloquent example of a functionally graded structure;[30] the dermal scales of *P. senegalus*,[3] comprised of multiple layers with graded properties, are serving as inspiration for armor. In this study, we demonstrate that the dermal layer of the *Arapaimas* belongs to this class of natural materials which will inspire scientists in the development of new systems, expanding the design principles of functionally graded structures.[31]

The structure of the *Arapaimas* scale, the largest fresh-water fish, is a graded composite with a highly mineralized surface and an interior composed of layers of parallel collagen fibers in a plywood/cross-lamellar pattern. The mineralized surface layer has corrugations that allow it to flex around the axis of the ridges without fracturing. This structural arrangement is unique and can serve as inspiration for the design of functionally graded composites with a ceramic surface. The corrugations create regions where the mineral thickness is reduced to a fraction of the maximum value and thus allow the brittle component to undergo significant flexure while retaining its integrity. The cracks observed in Figure 3 were produced when the scales were completely desiccated and are not representative of the hydrated scales.

In our study, we only considered the indentation behavior of a single scale. However, in real systems, the interaction between scales needs to be considered. Vernerey and Barthelat[32] reported that the fish scale structure will redistribute the deformation over a large region due to the strain-stiffening response, until the indented scale fractures. This strain-stiffening response minimizes the force concentration to prevent structural damage and failure.

We have characterized the structure and mechanical response of the *Arapaimas* scales and piranha teeth. By conducting penetration experiments into the scale using real piranha teeth, we showed that while they can penetrate into the light (covered) portion of the scale, they cannot enter into the dark (exposed) portion of the scale. The scale exterior is highly mineralized and the resistance to penetration is much higher than the bite force of the piranha and is such that the teeth fracture before penetration is completed.

Received: April 4, 2011
Final Version: November 3, 2011
Published online: January 9, 2012

[1] M. E. Launey, E. Munch, D. H. Alsem, H. D. Barth, E. Saiz, A. P. Tomsia, R. O. Ritchie, *Acta Mater.* **2009**, *57*, 2919.
[2] E. Munuch, M. E. Launey, D. H. Alsem, E. Saiz, A. P. Tomsia, R. O. Ritchie, *Science* **2008**, *322*, 1515.
[3] B. J. F. Bruet, J. Song, M. C. Boyce, C. Ortiz, *Nat. Mater.* **2008**, *7*, 748.
[4] J. Song, C. Ortiz, M. C. Boyce, *J. Mech. Behav. Biomed. Mater.* **2010**, *4*, 699.
[5] F. G. Torres, O. P. Troncoso, J. Nakamatsu, C. J. Grande, C. M. Gomez, *Mater. Sci. Eng., C* **2008**, *28*, 1276.
[6] T. Ikoma, H. Kobayashi, J. Tanaka, D. Walsh, S. Mann, *J. Struct. Biol.* **2003**, *142*, 327.
[7] A. Bigi, M. Burghammer, R. Falconi, J. H. Koch, S. Panzavolta, C. Riekel, *J. Struct. Biol.* **2001**, *136*, 137.
[8] H. Onozato, N. Watabe, *Cell Tissue Res.* **1979**, *201*, 409.
[9] L. Zylbergberg, J. Bereiter-Hahn, J. Y. Sire, *Cell Tissue Res.* **1988**, *253*, 597.
[10] L. Zylbergberg, J. Bonaventure, L. Cohen-Solal, D. J. Hartmann, J. Bereiter-Hanh, *J. Cell Sci.* **1992**, *103*, 273.
[11] G. Nicolas, F. Gaill, L. Zylbergberg, *J. Histochem. Cytochem.* **1997**, *45*, 119.
[12] L. Zylbergberg, G. Nicolas, *Cell Tissue Res.* **1982**, *223*, 349.
[13] O. P. Olson, N. Watabe, *Cell Tissue Res.* **1980**, *211*, 303.
[14] E. P. Popov, *Engineering Mechanics of Solids*, Prentice Hall, **1990**.
[15] Y.-S. Lin, C. T. Wei, E. A. Olevsky, M. A. Meyers, *J. Mech. Behav. Biomed. Mater.* **2011**, *4*, 1145.
[16] M. A. Meyers, A. Y. M. Lin, Y. S. Lin, E. A. Olevsky, S. Georgalis, *J O M* **2008**, 19.
[17] I. Sasagawa, M. Ishiyama, H. Yokosuka, M. Mikami, T. Uchida, *Mater. Sci. China* **2009**, *3*, 174.
[18] T. Atkins, *Eng. Fract. Mech.* **2006**, *73*, 2523.
[19] T. Atkins, *The Science and Engineering of Cutting*, Butterworth-Heinemann, **2009**, p. 230.
[20] R. Abu Al-Rub, *Mech. Mater.* **2007**, *39*, 787.
[21] M. W. Westneat, *J. Theor. Biol.* **2003**, *223*, 269.
[22] R. Mc. N. Alexander, *J. Linn. Soc.* **1964**, *45*, 169.
[23] T. Maie, H. L. Schoenfuss, R. W. Blob, *J. Morphol.* **2009**, *270*, 976.
[24] R. Mara, P. J. Motta, D. R. Huber, *J. Exp. Zool.* **2010**, *313*, 95.
[25] M. Akao, H. Aoki, K. Kato, *J. Mater. Sci.* **1981**, *16*, 809.
[26] R. G. Craig, F. A. Peyton, D. Sc, *J. Dent. Res.* **1958**, *37*, 710.
[27] D. R. Huber, M. N. Dean, A. P. Summers, *Interface* **2008**, *5*, 941.
[28] Miserez, S. S. Wasko, C. F. Carpenter, J. H. Waite, *Nat. Mater.* **2009**, *8*, 910.
[29] C. Weaver, Q. Wang, D. Kisailus, *Mater. Today* **2010**, *13*, 42.
[30] Miserez, T. C. Sun, F. W. Zok, J. H. Waite, *Science* **2008**, *318*, 1817.
[31] S. Suresh, A. Mortensen, Institute of Materials, London **1998**.
[32] F. J. Vernerey, F. Barthelat, *I.J.S.S.* **2010**, *47*, 2268.
[33] P.-Y. Chen, J. Schirer, A. Simpson, R. Nay, Y.-S. Lin, W. Yang, M. I. Lopez, J. Li, E. A. Olevsky, M. A. Meyers, *JMR* **2012**, *27*, in press.
[34] L. Melfi, ''Arapaima gigas'' (On-line), Animal Diversity Web. 2003. Accessed October 12, 2011, http://animaldiversity.ummz.umich.edu/site/accounts/information/Arapaima_gigas.html.

